Mg-Based Nanocomposites with High Capacity and Fast Kinetics for Hydrogen Storage

Xiangdong Yao,[†,‡] Chengzhang Wu,[§] Aijun Du,[†,⊥] Gao Qing Lu,[*,†] Huiming Cheng,[§] Sean C. Smith,[†,⊥] Jin Zou,[#] and Yinghe He[‡]

ARC Centre for Functional Nanomaterials, The University of Queensland, St. Lucia, QLD 4072, Australia, School of Engineering, James Cook University, Townsville, QLD 4811, Australia, National Laboratory of Materials Science, Institute of Metal Research, Shenyany 110015, China, Centre for Computational Molecular Science, Chemistry Building No. 68, The University of Queensland, QLD 4072, Brisbane, Australia, and Centre for Microscopy and Microanalysis and School of Engineering, The University of Queensland, St. Lucia, QLD 4072, Australia

Received: December 27, 2005; In Final Form: April 24, 2006

Magnesium and its alloys have shown a great potential in effective hydrogen storage due to their advantages of high volumetric/gravimetric hydrogen storage capacity and low cost. However, the use of these materials in fuel cells for automotive applications at the present time is limited by high hydrogenation temperature and sluggish sorption kinetics. This paper presents the recent results of design and development of magnesium-based nanocomposites demonstrating the catalytic effects of carbon nanotubes and transition metals on hydrogen adsorption in these materials. The results are promising for the application of magnesium materials for hydrogen storage, with significantly reduced absorption temperatures and enhanced ab/desorption kinetics. High level Density Functional Theory calculations support the analysis of the hydrogenation mechanisms by revealing the detailed atomic and molecular interactions that underpin the catalytic roles of incorporated carbon and titanium, providing clear guidance for further design and development of such materials with better hydrogen storage properties.

Introduction

Magnesium and magnesium-based alloys are among the most attractive materials for hydrogen storage because of their low cost and high capacity. With hydrogen, magnesium can form a hydride MgH_2 with a nominal 7.6 wt % of hydrogen, a complex hydride Mg_2FeH_6 with the highest known volumetric hydrogen density of 150 kg m^{-3} (more than double that of liquid hydrogen[1]), and $Mg(BH_4)_2$ with a very high theoretical capacity about 14.8 wt % of hydrogen. However, magnesium−hydrogen materials have limited practical application so far because both hydrogenation and dehydrogenation reactions are very slow and hence relatively high temperatures are required.[2−4] Fundamentally, to achieve high storage capacity at low system weight requires strong chemical bonding and light and stable stroage materials. However, to achieve fast cycling requires weak chemical bonding, fast kinetics, and less diffusion resistance, as might be found in surface adsorption. This constitutes a tradeoff between high capacity and fast kinetics.

Nanostructured materials offer some promises for storing hydrogen with high capacity and fast cycling at relatively low temperatures. The intrinsically large surface areas of nanophase catalysts can assist the dissociation of gaseous hydrogen, and the small volume of individual nanoparticles produces short diffusion paths to the materials' interiors. The charge and discharge cycle is a complex process that involves molecular dissociation, diffusion, and chemical bonding. Nanosized magnesium particles in conjunction with effective catalysts can overcome the high energy barrier of hydrogenation encountered in the bulk phase thus facilitating hydrogen absorption and transport.[5,6] Through nanostructuring with suitable catalysts, it may be possible for hydrogenation to occur at a low temperature with rapid kinetics. Such nanostructured Mg and its alloys synthesized by high-energy ball milling have recently been reported.[5,7−11] Zaluski et al. [5] found that addition of Pd significantly enhanced the hydrogen absorption/desorption kinetics. In a search for cheaper catalysts than Pd, other metals were studied. A MgH_2−5 wt % V nanocomposite was found to exhibit rapid hydrogenation kinetics where vanadium serves as a catalyst but in much larger quantity compared to Pd catalyst.[6] Previous studies[6,12] reported that iron (Fe) and titanium (Ti) were individually effective for enhancing hydrogen kinetics in Mg alloys. It is economically important to replace Pd by FeTi catalysts. Addition of both Fe and Ti may possibly be more effective than adding Fe or Ti separately as they could produce a synergetic catalytic effect. By high-energy ball milling of Fe and Ti together with Mg, for example, intermetallic FeTi could be formed and was demonstrated to also markedly improve the kinetics of Mg alloys.[9,13]

Due to their high specific surface area and unique adsorbing properties, nanostructured carbons synthesized by the hard templating method such as CMK-5 have been shown to have high catalytic dispersion and activity,[14] and could be used for carrying nanoscale metal catalyst to be milled into MgH_2. Carbon nanotubes have also been extensively studied for hydrogen storage.[15,16] Both mesoporous carbons and carbon nanotubes have high surface area and consist of grapheme

* Address correspondence to this author. E-mail: maxlu@uq.edu.au.
† ARC Centre for Functional Nanomaterials, The University of Queensland.
‡ James Cook University.
§ Institute of Metal Research.
⊥ Centre for Computational Molecular Science, The University of Queensland.
Centre for Microscopy and Microanalysis and School of Engineering, The University of Queensland.

10.1021/jp057526w CCC: $33.50
Published on Web 05/26/2006

sheets. In our previous study, it was found that Mg-nanostructured C nanocomposites obtained by milling graphite with Mg had significantly increased capacity of hydrogen storage.[17] However, the mechanisms of the metallic catalysts and nanocarbon additives remain unclear, which hinders the development of novel Mg-base nanocomposites with the desired hydrogen storage properties. Thus, it is desirable to understand at the nanoscale the effects of catalysts, defects, grain boundaries, interface boundaries, and impurity atoms.

Density functional theory (DFT) calculations have shown considerable power for the analysis of catalytic mechanisms.[18] Much insight can be gained for the process of designing alloy catalysts just from first principle calculations.[19] To date, only relatively few calculations of the dissociative chemisorption of H_2 onto a clean magnesium surface have been performed. [20−22] The energetically favored pathway and the activation barrier have been reported for this process. To clarify the recent experimental results and improve the hydrogenation performance of magnesium-based materials, we investigated the role of carbon and transition metal catalysts in the dissociation of H_2 on Mg(0001) surfaces and the diffusion of atomic H from Mg surface into the subsurface.

The present paper aimed to develop novel Mg-based nanocomposites with nanoscale metal catalysts such as iron (Fe) and titanium (Ti) particles that are promising in enhancing the kinetics of hydrogen uptake and release, and carbon nanotubes (CNTs) that could improve ambient hydrogen storage capacity by its unique structure. We report the experimental results of hydrogen sorption properties of Mg−FeTi (milled for 30 and 60 h, respectively) and Mg−FeTi−CNTs nanocomposites to investigate the catalytic mechanisms of FeTi and CNTs on hydrogenation/dehydrogenation of Mg. We also discuss in detail the correlations between our experimental observations and the results of recent ab initio density functional theory (DFT) calculations. These computational studies have demonstrated the catalytic effects on the dissociative chemisorption and diffusion of hydrogen on a Mg(0001) surface when titanium and carbon are respectively incorporated into Mg materials, and are very helpful in understanding the Mg−metal and Mg−C interactions and their effects on the hydriding process. [23−25]

Experimental and Theoretical Procedures

Experimental Details. All experiments and manipulations were carried out in a glovebox under an argon atmosphere.

Sample Preparation. MgH_2 was obtained by heating Mg powders (purchased for Lancaster) to 400 °C in a hydrogen storage rig. Then 90 wt % of the Mg powders was hydrided according to the volumetric calculations. Nano-Fe was made at the Institute of Metals Research, Chinese Academy of Sciences and the average grain size was about 100 nm. Ti was a commercial product from Aldrich Co, and CNTs was prepared and purified in our labs. The MgH_2−FeTi sample was mixed in the composition of MgH_2−5.0 wt % (2Fe + Ti), and mechanically milled by using a Spex 8000 ball mill. A hardened steel crucible and six steel balls 12 mm in diameter were used for the milling. The ball to powder weight ratio was 12.5:1. One gram of the powder was removed after 30 and 60 h of milling, respectively. The rest of the powder was then milled with 5.0 wt % of single-wall carbon nanotubles for an additional 10 h. The samples were then used for hydrogen property tests and microstructure characterization.

Microstructure and Hydrogenation Property Characterization. All samples were characterized by X-ray diffraction (XRD) analysis with a Cu Kα source. Their microstructures were characterized on a JEOL 2010 transmission electron microscope (TEM) operating at 200 keV. The hydrogen storage capability of these samples was evaluated by an in-house built automatic Sieverts apparatus, which measures the pressure and temperature simultaneously, so that we can measure the pressure change as a function of time at different temperatures. Under an initial pressure of 2 MPa, the absorption rate was measured by monitoring the pressure drop as a function of time. The desorption kinetics was measured at 573 K in a vacuum (10^{-5} atmospheric pressure). First, the hydrogen in the as-prepared sample was completely desorbed at 350 °C. Then, the sorption/desorption was performed at different testing temperatures and data were collected. Almost no capacity and kinetics change was observed with sorption/desorption cycling in the present experiments.

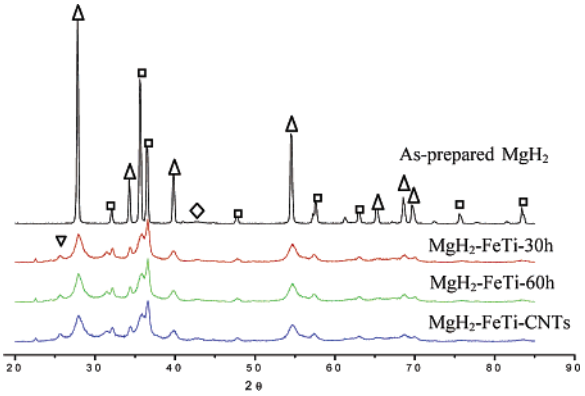

Figure 1. X-ray diffraction patterns: (△) β-MgH_2, (□) Mg, (◇) MgO, and (▽) γ-MgH_2.

Ab Initio Density Functional Theory (DFT). For convenient reference, we summarize the details of the DFT calculations reported previously,[23−25] the results of which are used as a basis for subsequent discussion and analysis in this work. The DFT calculations were performed with use of the plane-wave basis VASP code[26] implementing the generalized gradient approximation (GGA) of the PBE exchange correlation functional.[27] An all-electron description, the projector augmented wave method (PAW),[28] is used to describe the electron−ion interaction. The cutoff energy for plane waves is chosen to be 500 eV for a very accurate energy calculation. To determine dissociation barriers and minimum energy paths (MEP), the NEB method was used.[29] This method involves optimizing a chain of images that connect the reactant and product state. Each image is only allowed to move into the direction perpendicular to the hypertangent. Hence the energy is minimized in all directions except for the direction of the reaction path. A damped molecular dynamics was used to relax ions until the force in each image are less than 0.02 eV/Å. The vacuum space is 16 Å, which is enough to guarantee a sufficient separation between periodic images.

Results and Discussion

X-ray Diffraction. X-ray diffraction was performed on as-prepared MgH_2, MgH_2−FeTi milled for 30 and 60 h, and MgH_2−FeTi−CNTs samples, respectively. The corresponding diffraction patterns are shown in Figure 1.

XRD of the as-prepared MgH_2 sample shows that MgH_2 is present in the β-MgH_2 phase with a certain amount of Mg phase and a tiny amount of MgO phase. We believe the Mg phase originated from the residue of the hydrogenation process, while the MgO phase was due to contamination of the sample with traces of water inside the glovebox.[28] XRD patterns of the three

TABLE 1: Grain Sizes of Investigated Mg-Based Materials Systems by Different Milling Times

	MgH_2 (10 h of milling)	MgH_2−5 wt % FeTi		MgH_2−5 wt % FeTi−5 wt % CNTs (additional 10 h of milling with CNTs
		30 h of milling	60 h of miling	
d_1 (nm)[a]	29.1	16.6	13.9	11.3
d_2 (nm)[a]	64.7	29.1	22.6	20.3

[a] d_1 and d_2 indicate the diameters of MgH_2 and residual Mg, respectively.

milled samples show the γ-MgH_2 metastable phase, instead of the β-MgH_2 phase. This result agrees with the previous study[30] that suggested the γ-MgH_2 produced during ball milling decomposes after the first hydrogen desorption. No phases of Fe, Ti, or C were detected, since the amount of these additives was too low to generate sufficient diffraction intensity if there exists any such phase.

Since the crystallite size and lattice strain in fine particles can be determined by using the X-ray peak broadening technique, we can estimate the particle sizes of milled samples. As shown in Figure 1, the XRD pattern of as-prepared MgH_2 has a very sharp diffraction peak, whereas it becomes broadened with increased milling time. Most commonly the crystallite size is determined by the Scherrer formula.[31] However, this technique only takes account of the effect of the small size but neglects the strain effect, thus the result is only useful for considering trends in the change of crystallite size with milling conditions. Considering a combination of both crystallite size and lattice strain, the relationship between the peak width and the two effects is governed by following equation:[32]

$$B\cos\theta = \frac{0.9\lambda}{d} + \eta\sin\theta$$

where B is the peak width at half the maximum intensity, θ is the Bragg angle, d is the crystallite size, λ is the wavelength of the X-radiation used, and η is the strain. Thus, when $B\cos\theta$ is plotted against $\sin\theta$, a straight line is obtained with the slop as η and the intercept as $0.9\lambda/d$. From these, we can calculate the crystallite sizes of MgH_2 (d_1) and Mg (d_2) for our samples as given by Table 1. The average size of Mg−FeTi−CNTs particles, for example, is about 11 nm, which agrees very well with that observed by TEM reported in the next section (Figure 3b), whereas the grain size calculated by the Scherrer formula is about 7.6 nm, which is much smaller. This indicates that the strain caused by lattice enlargement is remarkable in the ball milling process and suggests that the atoms of catalysts (Fe, Ti, and C) could incorporate into the Mg structure.

Structural Characterization. The particle size and grain size of milled samples was examined by TEM. Figure 2 shows the TEM images of milled samples and shows typical sizes of particles and grains in different samples. Particles in these three milled samples with similar particle sizes on the order of several hundred nanometers were selected to investigate the evolution of grain sizes. It is observed that their grain sizes are quite different, evidenced by their corresponding electron diffraction patterns. In the case of the 30 h milled sample [as shown in Figure 2a], the electron diffraction pattern of the particle showed few sets of electron diffraction patterns, indicating that the average grain size of this sample is in the range of a hundred nanometers. For the case of the 60 h milled sample [Figure 2b], the electron diffraction pattern of a particle gives a discontinued ring pattern, implying that the grain size has been reduced significantly with a further 30 h of milling when compared with the 30 h milled sample. Interestingly, the electron diffraction pattern of a typical particle found in the sample milled for 70 h shows a continued ring pattern, representing very fine grain

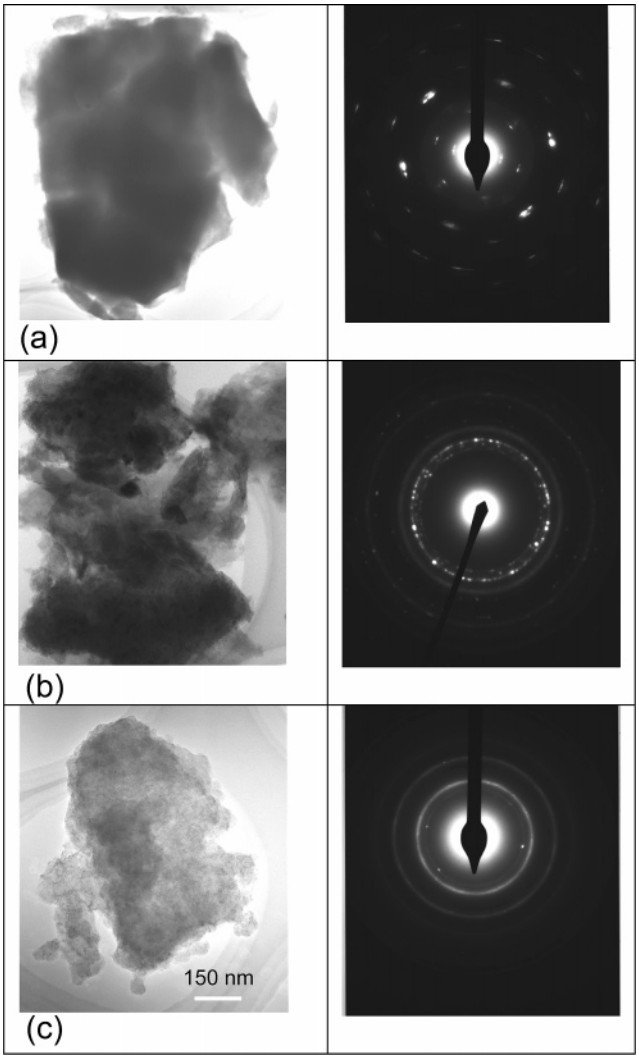

Figure 2. TEM images and electron diffraction patterns of (a) 30 h milled MgH_2−FeTi, (b) 60 h milled MgH_2−FeTi, and (c) MgH_2−FeTi−CNTs.

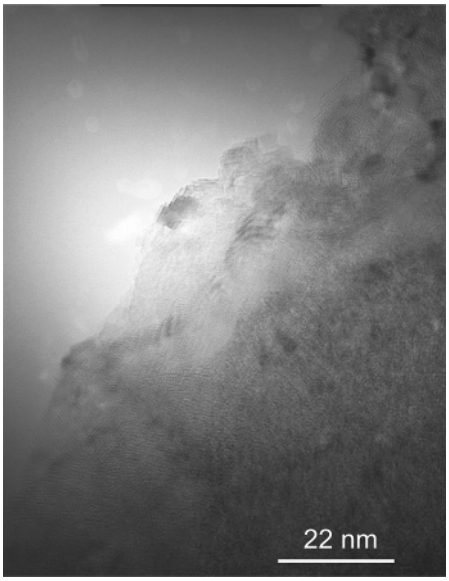

Figure 3. High-magnitude TEM image of the MgH_2−FeTi−CNTs sample.

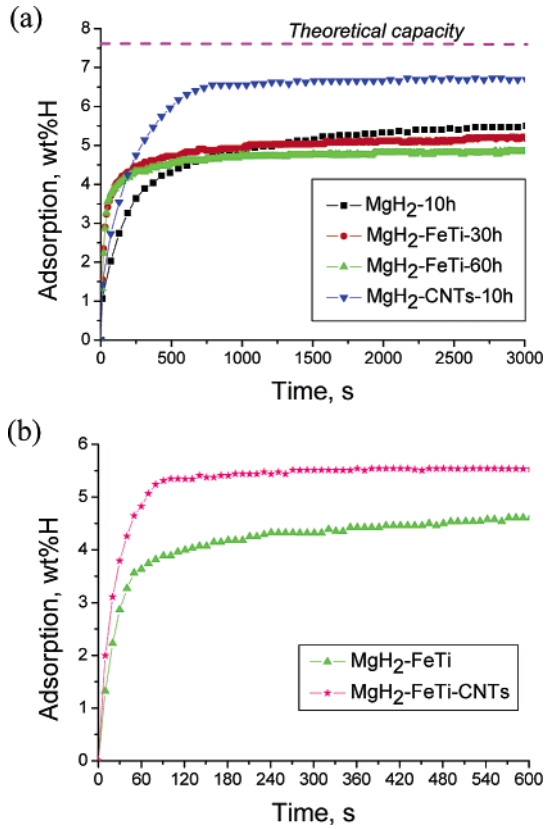

Figure 4. Hydrogen adsorption of several Mg-based systems at 300 °C and 2 MPa hydrogen pressure, in panel b Mg−FeTi was milled for 60 h and then CNTs was added for an additional 10 h of milling.

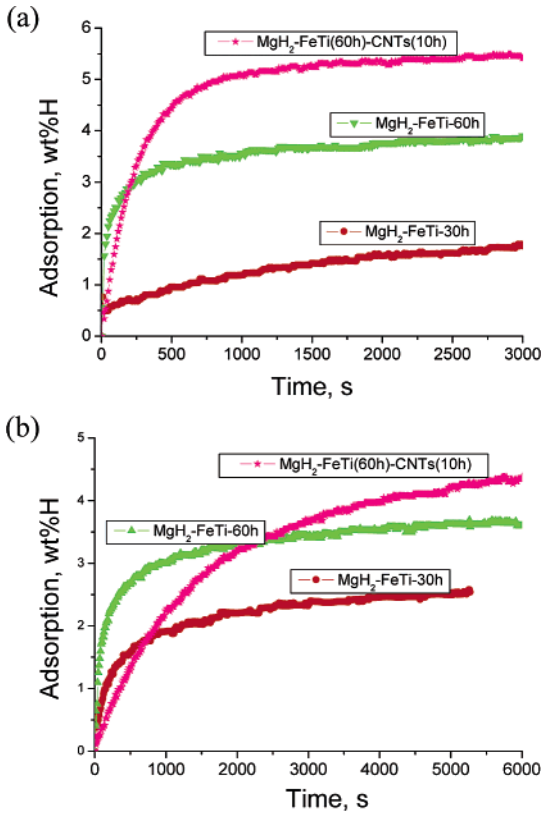

Figure 5. Hydrogen adsorption of Mg-based systems under 200 (a) and 150 °C (b) and 2 MPa hydrogen pressure.

sizes. Figure 3 is a TEM image of the sample milled for 70 h that shows detailed nanostructure. It is clearly seen that the average grain size is about 10 nm. Such composites with these microstructures are favorable for hydrogenation. It is remarkable that experimental results show that only 6% of Mg is not hydrogenated with a maximum capacity of 6.8 wt % of H. Apparently, the diffusion distance of hydrogen decreases significantly as the grain size decreases. This is the reason nanostructured materials can absorb a large amount of hydrogen.

Hydrogen Absorption. Figure 4 shows hydrogen absorption for MgH_2 (milled 10 h), MgH_2−FeTi (milled 30 and 60 h), and MgH_2−CNTs (milled 10 h) systems, respectively, under 300 °C and 2 MPa hydrogen pressure. It is seen that MgH_2 and MgH_2−FeTi samples absorbed similar amounts of hydrogen. The capacity is around 5 wt % of H within 3000 s. However, there is a significant difference in the absorption kinetics. The absorption rate of MgH_2−FeTi is remarkably faster, which reaches more than 90% of its maximum capacity within 1 min. However, there still exists a gap between the maximum capacity of these samples and the theoretical capacity in Mg. One possible reason is that the grain size of the materials is not uniformly small. Due to the difficulty in the ball milling processing of a ductile metal such as Mg, some of the grains may be larger than a certain threshold size beyond which hydrogenation is becoming limited. The hydrogenation process is limited by the growth of the hydride crystallites, which is controlled by the diffusion of hydrogen. The hydriding layer on the surface of magnesium is a barrier to this diffusion process.[5] That is, the hydrogenation rate of the remaining interior magnesium decreases with the increase of the hydriding layer thickness, and becomes virtually zero if the hydriding layer exceeds a critical thickness. Therefore, there exists a possibility to increase the maximum hydrogenation capacity and kinetics by reducing the grain size through modification of milling conditions and/or enhancing the hydrogen diffusion through introduction of more defects (diffusion channels). Figure 4 shows the effects of introducing CNTs into these materials. CNTs have been considered as attractive candidates and extensively studied for hydrogen storage because of their particular structures. It is reasonable to assume that the tubular structure could serve as a diffusion channel for hydrogen and significantly enhance the diffusion within metal hydrides if the tubular structure can be retained to some extend after ball milling with metals. Furthermore, carbon materials have been shown to have high catalytic dispersion and activity. They can therefore facilitate the ball milling of ductile metals to obtain finer grains (particles). The results shown in Figure 4 are promising and reveal that this concept as discussed above may be working. MgH_2−CNT reaches a maximum capacity of 6.8 wt % of H that is 1.8 wt % of H higher than that of MgH_2 under the same milling and hydrogenation conditions. Furthermore, the hydrogenation rate is also faster than that of MgH_2 but slower than that of the sample containing FeTi catalysts. We expect that CNTs and FeTi have a synergestic effect on the hydrogenation properties, e.g., increasing the capacity of MgH_2−FeTi without reducing the hydrogenation rate. It is also confirmed, as shown in Figure 4b, that adding CNTs increased the capacity of the MgH_2−FeTi system from 4.5 to 5.6 wt % of H within 10 min at 300 °C and made the kinetics better.

We investigated the hydrogen absorption property of MgH_2−FeTi milled for different times (30 and 60 h) and MgH_2−FeTi−CNTs, respectively, at low temperatures (200 and 150 °C), as shown in Figure 5. Figure 5a shows that the MgH_2−FeTi−CNTs composites display promising hydrogen absorption capacity and kinetics, reaching a capacity of 5.0 wt % of H within 10 min. The maximum capacity within 50 min is 5.5 wt % of H, which is much higher than that of the MgH_2−FeTi

system at 200 °C. Unlike the results at 300 °C, the milling time has a significant effect on the hydrogen uptake at low temperatures. MgH_2−FeTi milled for 60 h has a capacity of 3.8 wt % of H that is much higher that of the 30 h milled sample with a capacity of only 1.8 wt % of H, and also with much better kinetics at 200 °C. One reason is that the average grain size decreases with milling time under the present experimental conditions. The measurements of hydrogen absorption properties at 150 °C have the same trend as shown in Figure 5b. However, it is apparent that the hydrogenation rate is slower for the samples with CNTs additives, and shows that this effect becomes more evident as the hydrogenation temperature decreases. This phenomenon can be theoretically explained by changes of the energy barrier for hydrogen dissociation at the Mg surface and hydrogen diffusion into the sublayer and bulk magnesium.

Hydrogenation Mechanisms. It is generally regarded that the hydriding process is controlled by molecular hydrogen dissociation at the Mg surface and hydrogen diffusion into the Mg bulk. The hydrogen molecules must be dissociated into atoms as only atomic hydrogen can diffuse into Mg and form the metal hydride. Molecular hydrogen is too stable to be dissociated at normal temperatures because the energy for breaking the H−H bonding is very high. However, when molecular hydrogen approaches the metal surface the metal−H interaction will weaken the H−H bonding, thereby lowering the effective barrier for dissociation. Thus, the magnitude of the energy barrier for hydrogen dissociation on the surface reflects the strength of the metal−H interaction. Vegge[33] has previously calculated the hydrogen dissociation barrier on the pure Mg(0001) surface using DFT and reported the value was 1.15 eV. This value correlates to a hydrogenation temperature of about 400 °C, since the pure Mg can only be experimentally hydrogenated at such a temperature.[12] When other elements such as Ti, Fe, and C are introduced, the interactions between these elements, Mg, and hydrogen becomes more complicated and the energy barrier for hydrogen dissociation in this complex system will be one of the key points to understanding the hydrogenation mechanism of the Mg−metals−C nanocomposites.

As evidenced by XRD analysis in Figure 1, there are no traces of Fe, Ti, and C detected after ball milling with 5 (FeTi) and 5 wt % of CNT additives. This implies that it is possible for some of the added elements to be incorporated as atoms in the Mg structure through the high-energy ball milling process. With this possibility in mind, we carried out computational studies to examine the relaxed structures for incorporated Ti and C atoms in a Mg(0001) surface, as well as the impact this can have on the energy barrier for dissociative chemisorption of molecular hydrogen.[23−25] Our experimental results (Figure 4) demonstrated that a combination of Fe and Ti would be more effective on hydrogen absorption kinetics than Fe[12] or Ti[6] alone as we hypothesized; however, we could not find any single Fe, Ti, or FeTi intermetallics inside or on the surface of Mg. As DFT calculations for Fe-incorporated Mg are very difficult due to the magnetic and electronic structure of Fe, we only calculated the Ti-incorporated Mg surface to investigate the catalytic effect of transition metals on hydrogenation as an example. The results of these DFT studies[23,24] are reproduced in Figure 6. The barrier for hydrogen dissociation on the pure Mg(0001) surface is 1.05 eV, which agrees well with Vegge's result.[33] The calculated reaction path potential energy profile for a Ti-incorporated Mg surface is markedly different. There is an initial clustering of molecular hydrogen onto the Ti surface atom (0.6 eV exothermic), followed by dissociation with an activation barrier of only 0.103 eV. At the end of this reaction path the system is comprised of two H atoms located at surface sites adjacent to the incorporated Ti atom. The dramatic change in the reaction path energy profile when Ti is incorporated can be understood in terms of the strong interaction between the molecular orbital of H_2 and the metallic d orbital, involving a charge contribution from the s orbital of H_2 to the d orbital of Ti.[34] These results hence indicate that introduction of Ti into Mg will significantly decrease the energy barrier of hydrogen dissociation and possibly enable hydrogenation at low temperatures, a conclusion that is supported by experimental results.

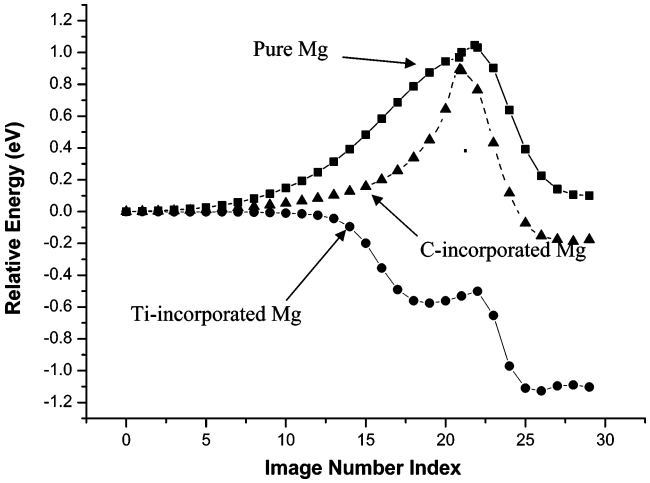

Figure 6. Hydrogen dissociation at the Mg(0001) surface: energy barrier for pure Mg and C-incorporated Mg(0001) surface and the minimum-energy-pathway profile.

We discussed the hypothesis as above that the carbon additive plays a physical role in facilitating the ball milling process to create finer particles with superior hydrogen absorption properties. Intriguingly, the recent DFT calculations indicated the possibility of an additional chemical catalytic role for carbon in enhancing hydrogen absorption.[24,25] Structural relaxation calculations showed that, up to quite high initial surface coverages of 0.5 or more, atomic carbon prefers to migrate into fcc interstitial sites in the first sublayer. This is accompanied by charge donation from surrounding Mg atoms to the sublayer C atoms, creating clusters of Mg atoms with partial positive charge. This phenomenon does not, however, have much effect on the energetics of surface dissociation of molecular hydrogen. Rather it appears to significantly enhance surface migration and diffusion of atomic H. The results shown in Figure 6 illustrate that the activation barrier for H_2 dissociation on Mg(0001) with an ideal subsurface of monolayer C atoms is just 0.16 eV smaller than that on the pure Mg(0001) surface, suggesting that C is likely to enhance the hydrogen dissociation kinetics significantly only at higher temperatures. At lower temperatures, a minor change to the hydrogen dissociation barrier would have little impact on the kinetics. Therefore, the kinetics is also being enhanced with adding CNTs as more sites (both Mg−metal and Mg−C interface) are available for hydrogen dissociation at a high temperature of 300 °C. However, at low temperatures the Mg−C interface becomes unfunctional for the hydrogen dissociation. This will lead to a smaller number of sites for hydrogen dissociation as the carbon atoms occupied the sites which were previously for the metal catalyst atoms. Accordingly, the hydrogenation kinetics slows down at low temperatures. Diffusion of the dissociated hydrogen atoms into the subsurface fcc sites through the fcc channels[33,35] is thought to be the most plausible route for H atoms into the bulk. The calculated

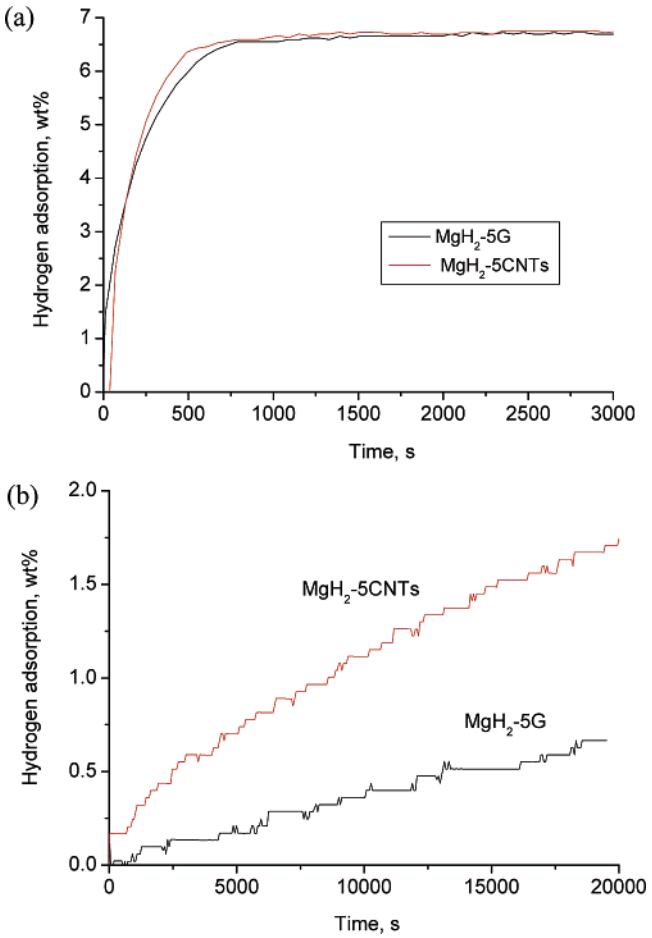

Figure 7. Hydrogen adsorption in Mg−CNTs and Mg−G samples at 300 (a) and 150 °C (b).

variation of diffusion barrier with and without C atoms incorporated indicated that the diffusion barrier is significantly decreased with C−Mg interactions. The electronic distribution around Mg atoms has been changed to form a channel that facilitates hydrogen atoms moving into the sublayer.[24,25] This represents an important alternative catalytic mechanism by which the CNT additives may increase the hydrogenation capacity of the Mg−CNTs system, because the enhancement of hydrogen diffusion enables more Mg to be transformed into hydride and hence the fraction of residual Mg becomes smaller.

Besides the catalytic effect on H diffusion of incorporated C atoms discussed above, the tubular structure of CNTs could in principle also facilitate hydrogen diffusion by allowing the hydrogen atoms to penetrate through their hollow tubes. Alternatively, if the tubes are filled by Mg/MgH_2, the net energy change in a hydrogen ab/desorption process will be reduced by as much as half the bulk value, which implies that the hydrogen diffusion is also enhanced.[36] However, for such possible mechanisms to be operational it would be necessary that the unique tubular structure of CNTs retains at least some of its structural integrity after high-energy ball milling. To check the existence of CNTs in Mg−CNTs samples after 10 h of ball milling, we design comparable experiments that test the hydrogen absorption properties of Mg−5 wt % G (graphite) by the same experimental conditions as the Mg−CNTs sample. The hydrogen absorption properties of these two samples at 300 and 150 °C, respectively, are shown in Figure 7. At temperature as high as 300 °C, the hydrogen absorption capacity of the Mg−G and Mg−CNTs is the same and the kinetics of the Mg−CNTs sample is a little better. However, there are significant

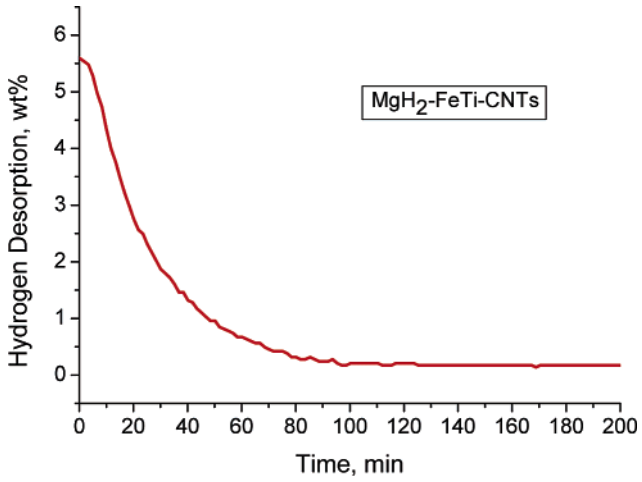

Figure 8. Hydrogen desorption of the MgH_2−5% FeTi−5% CNTs system at 300 °C.

differences in absorption properties of these two systems at 150 °C. Both the capacity and kinetics of Mg−CNTs are much better. These experimental results suggest that the atomic C effectively facilitates the hydrogen diffusion within Mg bulk at high temperature so the graphite and CNTs have the same effects on hydrogen absorption as they play the same role to supply atomic C when ball milling. However, at low temperature, the effect of residual CNTs becomes evident because the effect of atomic C by reducing the diffusion energy barrier weakens as the temperature decreases whereas the hydrogen atoms moving through the hollow tubes are not affected by temperature variation as they do not need energy. These results are therefore suggestive that both atomic C and residual CNTs exist in ball milled Mg−CNTs and both play an important role in hydrogen diffusion. The CNT additives are seen to have a greater effect on hydrogen sorption properties than graphite, especially at low temperatures.

The other possible reason alluded to above is that CNTs might serve as milling media that benefits ball milling, and subsequently, smaller particles (grains) have been formed to improve the hydrogen diffusion as the shorter diffusion distance. The TEM images confirm that the Mg milled for 30 h has an apparently textile structure (a typical structure of milled ductile materials shows that the materials have not been well milled into fine powders) and Mg−FeTi−CNTs shows much finer particles (grains). The difference in the capacity as given in Figures 4 and 5 between Mg−FeTi and Mg−FeTi−CNT systems may therefore arise from some combination of physical ball milling effects that produce smaller grain sizes and the chemical catalytic role of incorporated carbon (and possibly also residual CNT structures) in enhancing H diffusion.

Hydrogen Desorption. It has been reported that fast dehydrogenation reaction kinetics in Mg can be achieved by using a catalyst in the form of metallic nanoparticls dispersed at the Mg surface.[37] The metallic nanoparticles favor the hydrogen dissociation and atomic C enhances the jump of H atoms toward the subsurface layers, which might also facilitate the diffusion of H atoms from the broken Mg−H bonding of MgH_2 toward the Mg surface and the recombination of the H atoms into hydrogen molecules. This is supported by the result shown in Figure 8. Fast desorption kinetics at a relatively lower temperature of 300 °C has been achieved in catalyst-doped MgH_2 (catalysts: Ti, Fe, and C) by using ball milling. MH_2 with doped nanoscale FeTi and C can be dehydrided at 300 °C within 80 min. The result suggests a catalytic role of the additives (Fe, Ti, and C) dispersed in the Mg grains on the hydrogen

desorption kinetics but the mechanisms are far from fully understood, which will be a further topic of research both theoretically and experimentally.

Conclusions

Investigations of ball milling conditions such as milling time and different additives have been performed to study the microstructure evolution and its effect on hydrogenation absorption properties. With increasing milling time, the average crystallite size of grains decreases, which significantly enhances both the hydrogen absorption capacity and kinetics. However, the grains produced by the ball milling technique are not uniform. There exist some large grains that cannot be fully hydrided, leading to a gap between the real capacity and the theoretical capacity for hydrogen uptake. One of the benefits for adding CNTs is to increase the milling efficiency to produce finer and more uniform grains (in small particles) since CNTs serve as dispersive media.

Combinations of Fe and Ti serve as effective catalysts for hydrogen dissociation at the Mg surface, as evidenced by the very good hydrogen absorption kinetics observed for the MgH_2−FeTi nanocomposites tested in this study. These results offer substantial promise that further development of effective catalysts can enable fast hydrogen absorption at lower temperatures. The detailed investigation of these effects by first-principle calculations reveals that the doped metals such as Ti significantly decrease the energy barrier of hydrogen dissociation at the Mg surface, enabling hydrogen absorption at low temperatures with fast kinetics. The doped C plays a minor role in hydrogen dissociation on the surface, but remarkably facilitates hydrogen diffusion into subsurface layers, which enhance the magnesium hydrides formation to increase the real hydrogen storage capacity.

Catalyst (Fe, Ti, and C)-doped Mg by ball milling also improves the dehydrogenation of MgH_2. The magnesium hydrides can be dehydrided at 300 °C with reasonable kinetics. Further studies of the catalytic mechanism will be performed to provide a tool for searching for more effective catalysts that enable ab/desorption at lower temperatures.

Acknowledgment. Financial support from the Australian Research Council and the National Science Foundation of China is gratefully acknowledged. Generous grants of high-performance computer time from both the Computational Molecular Science cluster computing facility at The University of Queensland and the Australian Partnership for Advanced Computing (APAC) National Facility are also acknowledged.

References and Notes

(1) Seayad, A. M.; Antonelli, D. M. *Adv. Mater*. **2004**, *16*, 765.

(2) Louis, S Hydreogen in Intermetallic Compounds I. In *Topics in Applied Physics*; Springer: Berlin, Germany, 1988; Vol. 63, p 350.

(3) Schlapbach, L.; Zuttel, A. *Nature* **2001**, *414*, 353.

(4) Gutfleisch, O.; Schlorke-de Boer, N.; Ismail, N.; Herrich, M.; Walton, A.; Speight, J.; Harris, I. R.; Pratt, A. S.; Zuttel, A. *J Alloys Compd.* **2003**, *356*−*357*, 598.

(5) Zaluski, I.; Zaluska, A.; Tessier, P.; Strom-Olsen, J. O.; Schulz, R. *Mater. Sci. Forum* **1996**, *225*, 853.

(6) Liang, G.; Boily, S.; Huot, J.; Van Neste, A.; Schulz, R. *J Alloys Compd*. **1998**, *268*, 302.

(7) Berlouis, L. E. A.; Cabera, E.; Hall-Barientos, E.; Hall, P. J.; Dodd, S. B.; morris, S.; Imam, M. A. *J. Mater. Res.* **2001**, *16*, 45.

(8) Liang, G, *J. Alloys Compd.* **2004**, *370*, 123.

(9) Mandal, P.; Srivastava, O. N. *J. Alloys Comput.* **1994**, *205*, 111.

(10) Fujii, H.; Orimo, S. *Phys. B* **2003**, *328*, 77.

(11) Orimo, S.; Fujii, H. *Appl. Phys. A* **2001**, 72, 167.

(12) Zaluski, I.; Zaluska, A.; Strom-Olsen, J. O. *J. Alloys Compd*. **1999**, *288*, 217.

(13) Wang, P.; Wang, A. M.; Ding, B. Z.; Hu, Z. Q. *J. Alloys Compd.* **2002**, *34*, 243.

(14) Joo, S. H.; Choi, S. J.; Ryoo, R. et al. *Nature* **2001**, *412*, 169.

(15) Dillon, A. C.; Jones, K. M.; Bekkedahl, T. A.; Kiang, C. H.; Bethune, D. S.; Heben, M. J. *Nature* **1997**, *386*, 377.

(16) Lin, J. *Science* **2000**, *287*, 939.

(17) Wu, C. Z.; Wang, P.; Yao, X.; Lu, G. Q.; Chen, H. M. *J Phys. Chem. B* **2005**, *109*, 22217

(18) Greeley, J.; Norskov, J. K.; Mavrikakis, M. *Annu. Rev. Phys. Chem*. **2002**, *53*, 319.

(19) Vang, R. T.; Honkala, K.; Dahl, S.; Vestergaard, E. K.; Schnadt, J.; Egsgaard. E.; Clausen, B. S.; Norskov, J. K.; Besenbacher, F. *Nature Mater.* **2005**, *4*, 160.

(20) Norskov, J. K.; Houmoller, A. M. *Phys. Rev. Lett.* **1981**, *46*, 257.

(21) Greeley, J.; Mavrikakis, M. *Nat. Mater.* **2004**, *3*, 810.

(22) Bird, D. M.; Clarke, L. J.; Payne, M. C.; Stich, I. *Chem. Phys. Lett.* **1993**, *212*, 518.

(23) Du, A. J.; Smith, S. C.; Yao X.; Lu, G. Q. *J. Phys. Chem. B* **2005**, *109*, 18037.

(24) Du, A. J.; Smith, S. C.; Yao X.; Lu, G. Q. *J. Phys. Chem. B* **2006**, *110*, 1814.

(25) Du, A. J.; Smith, S. C.; Yao X.; Lu, G. Q. *J. Phys. C Conf. Ser.* **2006**, *29*, 167.

(26) Kresse, G.; Furthmuller, J. *Comput. Mater. Sci* **1996**, *6*, 15.

(27) Perdew, J. P.; Burke, K.; Ernzerhof, M. *Phys. Rev. Lett.* **1996**, *77*, 3865.

(28) Kresse, G.; Joubert, D. *Phys. Rev. B* **1999**, *59*, 1758.

(29) Henkelman, J.; Jónsson, H. *J. Chem. Phys.* **2000**, *113*, 9978.

(30) Huot, J.; Liang, G.; Boily, S.; Van Neste, A.; Schulz, R. *J Alloys Compd.* **1995**, *293*−*295*, 495.

(31) Lonnberg, B. *J. Mater. Sci.* **1994**, *29*, 3224.

(32) Aymard, L.; Dehahaye-Vidal, A.; Portemer, F.; Disma, F. *J Alloys Compd.* **1975**, *30*, 227.

(33) Vegge, T. *Phys. Rev. B* **2004**, *70*, 035412.

(34) Nobuhara, K.; Kasai, H.; Dino, W. A.; Nakanishi, H. *Surf. Sci.* **2004**, *566*−*568*, 703.

(35) Jacobson, N.; Tegner, B.; Schröder, E.; Hyldgaard, P.; Lundqvist, B. I. *Comput. Mater. Sci.* **2002**, *24*, 273.

(36) Liang J.; Kung, W. C. *J. Phys. Chem. B* **2005**, *109*, 17837.

(37) Zaluska, A.; Zaluski, L.; Strom-Olsen, J. O. *Appl. Phys. A*: *Mater. Sci. Process.* **2001**, *72*, 157.